Energy levels and correlation crystal-field effects in Er^{3+}-doped garnets

John B. Gruber
Department of Physics, San Jose State University, San Jose, California 95192-0106

John R. Quagliano, Michael F. Reid,* and Frederick S. Richardson
Chemistry Department, University of Virginia, Charlottesville, Virginia 22901

Marian E. Hills and Michael D. Seltzer
Chemistry Division, Research Department, Naval Air Warfare Center Weapons Division, China Lake, California 93555-6001

Sally B. Stevens† and Clyde A. Morrison
Harry Diamond Laboratories, U.S. Army Laboratory Command, Adelphi, Maryland 20783

Toomas H. Allik
Science Applications International Corporation, 1710 Goodridge Drive, McLean, Virginia 22102
(Received 5 October 1992; revised manuscript received 1 June 1993)

The crystal-field energy-level structures of three different Er^{3+}-doped garnet systems are analyzed and compared in this study. The garnet hosts are $Y_3Al_5O_{12}$ (YAG), $Y_3Sc_2Al_3O_{12}$ (YSAG) doped with Tm^{3+} as a sensitizer ion, and $Y_3Sc_2Ga_3O_{12}$ (YSGG) doped with Cr^{3+} as a sensitizer ion. The focus is on energy levels assigned to Er^{3+} ions substituted for Y^{3+} at dodecahedral (D_2 symmetry) sites in the cubic garnet lattices. Analyses are carried out on experimental energy-level data that span up to 29 different $^{2S+1}L_J$ multiplet manifolds (between 0 and 44 000 cm^{-1}) of the Er^{3+} $4f^{11}$ electronic configuration. These data include the locations of 117 crystal-field levels of Er^{3+} in YAG, 109 levels of Er^{3+} in YSAG, and 92 levels of Er^{3+} in YSGG. The energy-level analyses are based on the use of a parametrized model Hamiltonian for the $4f^{11}$ electronic configuration of Er^{3+} in a crystal field of D_2 symmetry. The model Hamiltonian includes both atomic ("free-ion") and crystal-field interactions, parametrized to fit calculated eigenvalues to experimentally observed energies. The crystal-field part of the Hamiltonian is defined to include the standard one-electron interaction operators, as well as additional operators that provide a partial, phenomenological consideration of electron-correlation effects in the $4f$-electron–crystal-field interactions. The latter, *correlation crystal-field* (CCF) interactions, are introduced to address crystal-field splittings within several J-multiplet manifolds that are poorly represented by one-electron crystal-field interaction models. Inclusion of CCF terms in the model Hamiltonian leads to dramatic improvement in the fits between calculated and observed crystal-field splittings within the problematic multiplet manifolds. All of the energy-level analyses reported in this study were carried out within commensurate parametrization schemes, and the Hamiltonian parameters derived from these analyses provide a suitable basis for comparing the $4f$-electron–crystal-field interaction properties of Er^{3+} in YAG, YSAG, and YSGG. These analyses are based entirely on experimental data that specify the *locations* of energy levels, but do not provide any explicit information about the angular momentum (JM_J) compositions of the crystal-field wave functions.

I. INTRODUCTION

Trivalent erbium (Er^{3+},$4f^{11}$) can act either as an activator ion or as a sensitizer ion in a variety of midinfrared solid-state lasers.[1–14] Stimulated emission at visible wavelengths can also be achieved from Er^{3+} through various upconversion schemes.[14–20] Garnets containing Er^{3+} ions have been used successfully as midinfrared solid-state lasers, while Er^{3+}-doped fluorides with relatively smaller crystal fields and lower phonon energies (longer metastable lifetimes) are better suited as upconversion lasers.[19–23] Detailed spectroscopic studies provide information leading to an assessment of the lasing efficiency of Er^{3+} ions at different wavelengths in different crystals.[21] For many of the Er^{3+}-doped laser crystals, the spectroscopic analyses are incomplete.[24–29] In some cases, only parts of the multiplet structure of the $4f^{11}$ electronic configuration have been characterized, and in many cases detailed analyses of crystal-field splittings have been confined to a relatively small number of multiplet manifolds.[24,25]

In the present study, we examine the energy-level structure of Er^{3+} doped into three different garnet hosts: $Y_3Al_5O_{12}$ (YAG); $Y_3Sc_2Al_3O_{12}$ (YSAG) doped with Tm^{3+} as a sensitizer ion; and $Y_3Sc_2Ga_3O_{12}$ (YSGG) doped with Cr^{3+} as a sensitizer ion. We focus entirely on energy levels assigned to Er^{3+} ions substituted for Y^{3+} at dodecahedral (D_2 symmetry) sites in the cubic garnet lat-

0163-1829/93/48(21)/15561(13)/$06.00

tices. The main emphasis is on comparative energy-level analyses that reflect differences (and similarities) between Er^{3+} ($4f^{11}$) host-lattice interactions in the respective systems. The energy-level data included in our analyses span 29 $^{2S+1}L_J$ ($4f^{11}$) multiplet manifolds of Er^{3+} in YAG and YSAG, and 22 multiplet manifolds of Er^{3+} in YSGG. These data include the locations of 117 crystal-field levels of Er^{3+} in YAG, 109 levels of Er^{3+} in YSAG, and 92 levels of Er^{3+} in YSGG. All of these crystal-field levels are Kramers doublets of identical symmetry ($E_{1/2}$) in the D_2^* double group. The experimental data analyzed in this study provide information about the energies of the crystal-field levels, but they do not provide explicit information about the angular momentum (JM_J) properties of these levels.

Our energy-level analyses are based on the use of a parametrized model Hamiltonian for the $4f^{11}$ electronic state structure of Er^{3+} in a crystal field of D_2 symmetry. This model Hamiltonian includes both atomic ("free-ion") and crystal-field interactions, parametrized to fit the eigenvalues of the model Hamiltonian to experimentally observed energies. All analyses are carried out within commensurate parametrization schemes, and both the atomic and crystal-field Hamiltonian parameters derived from these analyses may be used to compare the interaction properties of Er^{3+} in YAG, YSAG, and YSGG.

The crystal-field part of our model Hamiltonian is defined to include the standard one-electron interaction operators, as well as additional operators that provide for some partial, phenomenological consideration of electron-correlation effects in the $4f$-electron–crystal-field interactions. Several J-multiplet manifolds of Er^{3+} in garnets (and in many other crystalline hosts) exhibit crystal-field splittings that cannot be accounted for by standard one-electron crystal-field interaction models. Similar problems are encountered in energy-level analyses of Nd^{3+} in a variety of crystalline hosts.[30–32] These problems are largely resolved by the inclusion of certain *correlation crystal-field* (CCF) interaction terms in the model Hamiltonian. Inclusion of the CCF interaction terms leads to dramatic improvement in the fits between calculated and observed crystal-field splitting energies within the problematic multiplet manifolds, and it also improves the *overall* agreement between calculated and observed energy levels. This suggests that CCF effects may be of essential importance in rationalizing the electronic energy-level structures of Nd^{3+} and Er^{3+} in crystalline hosts. However, it must be emphasized that neither the results presented here nor those reported previously can provide definitive evidence in this regard. In this study, CCF effects are considered entirely within a phenomenological context, and they are used to rationalize observed crystal-field splitting energies. The accuracies of the state vectors obtained from our CCF calculations cannot be tested with the experimental data available in this study. As was noted earlier, these data consist entirely of energy-level *locations* and do not provide information about the JM_J compositions of the crystal-field wave functions.

This is a comparative study of Er^{3+}-doped garnets in which energy-level analyses are carried out within commensurate parametrization schemes for both the atomic and crystal-field parts of the $4f$-electron Hamiltonian, and in which the energy-level data span up to 29 different J-multiplets of the Er^{3+} $4f^{11}$ electronic configuration. The Hamiltonian parameters derived from these energy-level analyses provide a basis for comparing Er^{3+} ($4f^{11}$)–crystal-field interactions in the YAG, YSAG, and YSGG host lattices. Furthermore, the eigenvectors of the parametrized model Hamiltonians should provide useful basis sets for future calculations of properties other than energy (e.g., optical transition probabilities and magnetic properties).

II. EXPERIMENTAL DETAILS

The crystals used in the present study, yttrium aluminum garnet (YAG), yttrium scandium aluminum garnet (YSAG), and yttrium scandium gallium garnet (YSGG), were grown by Kokta and Randles using the Czochralski method.[33–35] Based on a distribution coefficient of 0.96 and the dopant concentration in the melt, each crystal contained approximately 1 at.% erbium. The YSAG and YSGG crystals also contained a sensitizer ion (5 at.% thulium in YSAG, and 1 at.% chromium in YSGG).

We have been able to separate the Tm^{3+} ion spectra and the Cr^{3+} ion spectra from the Er^{3+} ion spectra in the wave-length regions where the spectra overlap. The spectra of Tm:YSAG is reported in a separate paper.[36] We identified the sharp-line spectra of Er^{3+} superimposed on the Cr^{3+} absorption bands by analyzing the Cr^{3+} spectra in the same way we carried out a detailed crystal-field splitting analysis of the energy levels of Cr^{3+} ions in YAG (Ref. 37) and in gadolinium scandium gallium garnet (Ref. 38).

Absorption spectra were recorded between 1.55 and 0.20 μm with a Cary Model 2390 spectrophotometer. Spectra were obtained at 4 K by mounting the crystal in a continuous-flow helium cryostat (Oxford, Model 1204D). At this temperature the first excited energy (Stark) level of the ground-state multiplet manifold of Er^{3+}, $^4I_{15/2}$, is largely unpopulated in the garnet hosts YAG (22 cm^{-1}), YSAG (21 cm^{-1}), and YSGG (33 cm^{-1}). The Er^{3+} spectra at 4 K were generally well resolved. Hot bands were observed in the absorption spectra at higher temperatures. An analysis of these hot bands led to the identification of many of the excited Stark levels of the $^4I_{15/2}$ multiplet manifold; this identification was confirmed by an analysis of the fluorescence data.

Fluorescence spectra at 4 K were obtained using a Nd^{3+}:YAG laser-pumped dye laser as the excitation source and a 0.85-m Spex double monochromator equipped with a photomultiplier. Fluorescence signals were recorded using a boxcar averager and a digital oscilloscope.

From an analysis of both the absorption and emission spectra, we conclude that most Er^{3+} ions substitute for Y^{3+} ions in dodecahedral sites having D_2 symmetry in the cubic garnet lattice.[33,35,39] The additional presence of Er^{3+} ions in C_{3i} sites and in disturbed dodecahedral sites

has received growing attention in recent years[28,35,40,41] as the basis of energy-transfer models developed to interpret the efficiency and tunability of laser output in the midinfrared.[21] The crystal-field splitting analyses reported in this paper concern only those Er^{3+} ions in D_2 sites.

With few exceptions, all $J+\frac{1}{2}$ Stark components of an isolated multiplet manifold $^{2S+1}L_J$ of Er^{3+} $(4f^{11})$ have been identified. The Stark levels of Er^{3+} are represented by the same symmetry label $(E_{1/2})$ in D_2 symmetry, and electronic electric-dipole and magnetic-dipole transitions are allowed between all Stark levels. The laser-induced fluorescence spectra shown in Figs. 1–4 illustrate the different crystal-field splittings of Er^{3+} ^4I_J multiplet manifolds observed in the three garnet hosts. The Stark levels of these manifolds are the most important levels associated with midinfrared laser emission.

III. ENERGY-LEVEL CALCULATIONS AND ANALYSIS

The energy-level structure of the $4f^{11}$ electronic configuration of Er^{3+} in garnet hosts is analyzed in terms of a parametrized model Hamiltonian that assumes a D_2 site symmetry for the Er^{3+} ions. This Hamiltonian is defined to operate entirely *within* the manifold of $SLJM_J$ angular momentum states associated with the $4f^{11}$ electronic (or the conjugate $4f^3$ "hole") configuration. All parts of the Hamiltonian that depend on $4f$-electron radial coordinates are represented as parameters that may be used as variables in experimental-to-calculated energy-level data fits. For convenience of discussion, we partition the parametrized model Hamiltonian as follows:

$$\hat{H}=\hat{H}_a+\hat{H}_{\rm cf}+\hat{H}_{\rm occf}\ , \tag{1}$$

where $\hat{H}_a$ denotes an "atomic" Hamiltonian defined to include all relevant interactions *except* those associated with components of the crystal field that are not spherically symmetric, and $\hat{H}_{\rm cf}$ and $\hat{H}_{\rm occf}$ are crystal-field interaction operators that are defined below. The atomic Hamiltonian is expressed explicitly as

$$\hat{H}_a=E_{\rm av}+\sum_k F^k\hat{f}_k+\alpha\hat{L}(\hat{L}+1)+\beta\hat{G}(G_2)+\gamma\hat{G}(R_7)$$
$$+\sum_i T^i\hat{t}_i+\zeta\hat{A}_{\rm s.o.}+\sum_k P^k\hat{p}_k+\sum_j M^j\hat{m}_j\ , \tag{2}$$

where $k=2,4,6$, $i=2,3,4,6,7,8$, and $j=0,2,4$. The parameters and operators in this expression are defined according to standard practice.[42,43]

The $\hat{H}_{\rm cf}$ operator is defined to represent the components of the *one-electron* crystal-field interactions that are not spherically symmetric. Only the *even-parity* parts of this operator are relevant to our $4f^{11}$ (Er^{3+}) electronic energy-level calculations, and if we assume D_2 symmetry for the crystal-field potential (at the Er^{3+} sites), we may

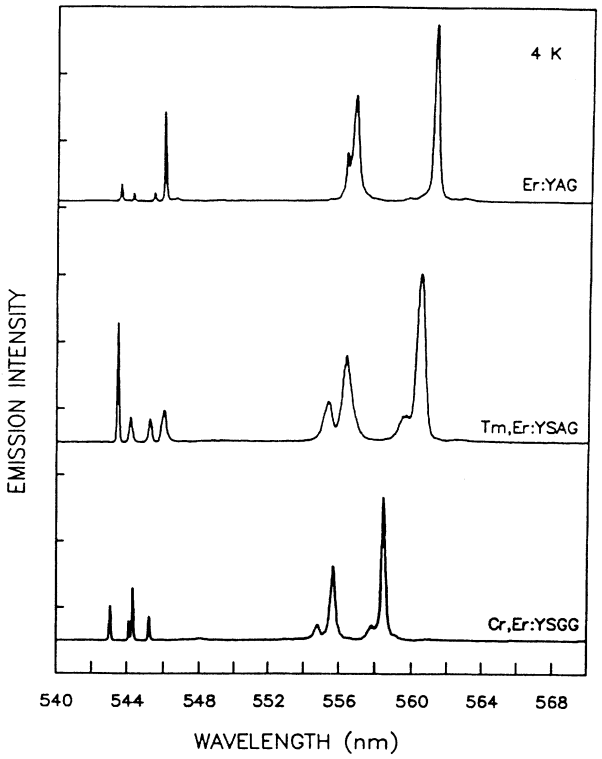

FIG. 1. Er^{3+} fluorescence from $^4S_{3/2}$ to $^4I_{15/2}$ following excitation of $^4F_{7/2}$ and subsequent nonradiative decay. Excitation wavelengths are 484.0 nm (Er:YAG), 487.8 nm (Tm,Er:YSAG), and 486.9 nm (Cr,Er:YSGG).

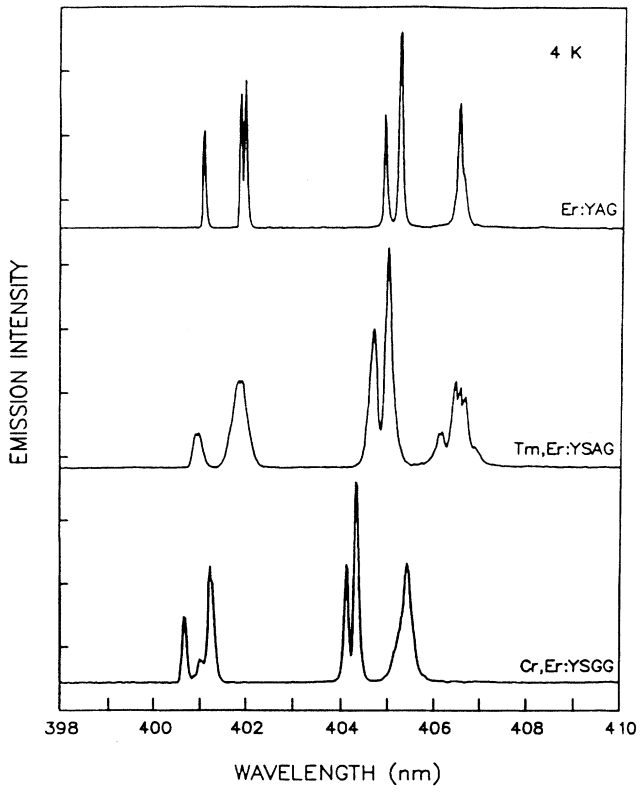

FIG. 2. Er^{3+} fluorescence from $^2P_{3/2}$ to $^4I_{13/2}$ following excitation of $^4G_{7/2}$ and subsequent nonradiative decay. Excitation wavelengths are 293.2 nm (Er:YAG), 293.0 nm (Tm,Er:YSAG), and 293.4 nm (Cr,Er:YSGG).

express $\hat{H}_{\rm cf}$ in the following form:

$$\hat{H}_{\rm cf}=\sum_{k,q} B_q^k \hat{U}_q^{(k)} \tag{3a}$$

$$=B_0^2\hat{U}_0^{(2)}+B_2^2[\hat{U}_2^{(2)}+\hat{U}_{-2}^{(2)}]+B_0^4\hat{U}_0^{(4)}+B_2^4[\hat{U}_2^{(4)}+\hat{U}_{-2}^{(4)}]+B_4^4[\hat{U}_4^{(4)}+\hat{U}_{-4}^{(4)}]$$
$$+B_0^6\hat{U}_0^{(6)}+B_2^6[\hat{U}_2^{(6)}+\hat{U}_{-2}^{(6)}]+B_4^6[\hat{U}_4^{(6)}+\hat{U}_{-4}^{(6)}]+B_6^6[\hat{U}_6^{(6)}+\hat{U}_{-6}^{(6)}]\,, \tag{3b}$$

where $\hat{U}_q^{(k)}$ is a unit-tensor operator (of rank k and order q) summed over all $4f$ electrons, and the B_q^k parameters contain the radially dependent parts of the one-electron crystal-field interactions.

The $\hat{H}_{\rm occf}$ operator in Eq. (1) is defined according to the prescriptions of Judd[44] and Li and Reid[30,45] to include contributions from correlated two-electron crystal-field interactions. In the parametrization scheme employed in the present study, $\hat{H}_{\rm occf}$ is formulated in terms of a set of orthogonal operators, and the subscript level on $\hat{H}_{\rm occf}$ stands for *orthogonal correlation crystal field*. In Judd's notation, the $\hat{H}_{\rm occf}$ operator is written[44,45]

$$\hat{H}_{\rm occf}=\sum_{iKQ} G_{iQ}^K \hat{g}_{iQ}^{(K)}\,, \tag{4}$$

where K runs through the even integers from 0 to 12, Q is restricted by crystal-field symmetry, the number of operators varies with K, and the label i is used to distinguish between different operators (with identical K's). Some of the terms in expression (4) are excluded from the $\hat{H}_{\rm occf}$ operator when it is used in Eq. (1). The excluded terms are those with $K=0$, which represent interelectronic Coulombic interactions already represented in the $\hat{H}_a$ operator, and those with $i=1$ ($K=2$, 4, and 6), which represent one-electron crystal-field interactions already represented in the $\hat{H}_{\rm cf}$ operator. After these terms are excluded from Eq. (4), there remain 40 different $G_i^K\hat{g}_i^{(K)}$ terms (not counting the number of Q components for each of the surviving terms).[30] This poses a serious dilemma in any attempt to use the $\hat{H}_{\rm occf}$ Hamiltonian in performing parametric analyses of experimental energy-level data. The number of parameters that can be used as independent "fitting" variables in these analyses is general-

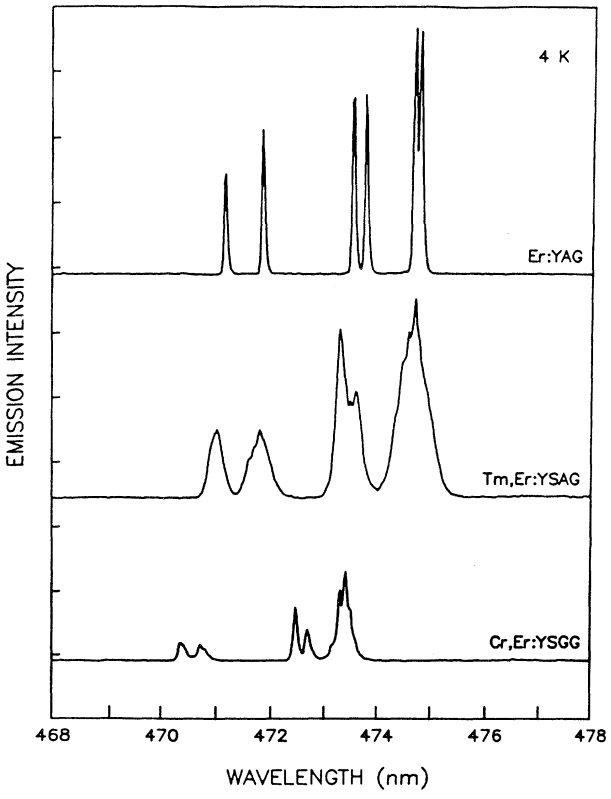

FIG. 3. Er^{3+} fluorescence from $^2P_{3/2}$ to $^4I_{11/2}$ following excitation of $^4G_{7/2}$ and subsequent nonradiative decay. Excitation wavelengths are 293.2 nm (Er:YAG), 293.0 nm (Tm,Er:YSAG), and 293.4 nm (Cr,Er:YSGG).

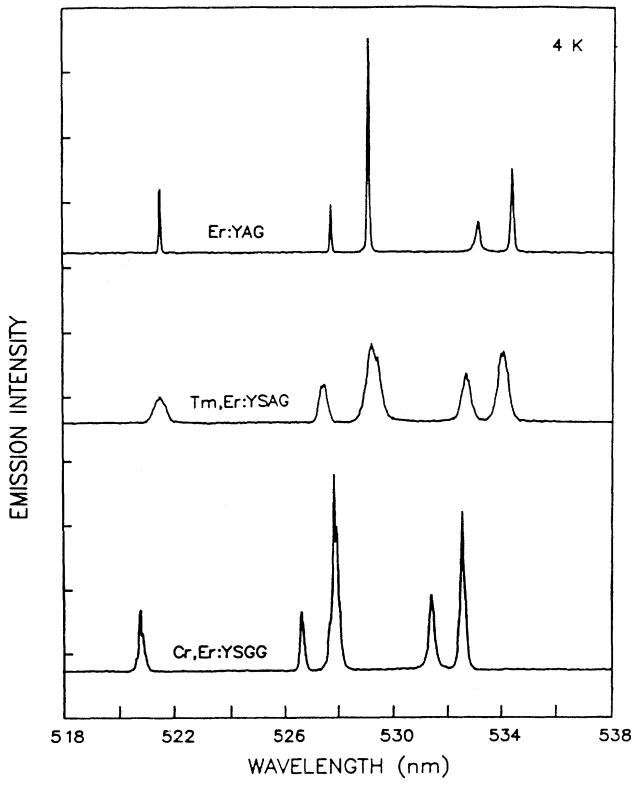

FIG. 4. Er^{3+} fluorescence from $^2P_{3/2}$ to $^4I_{9/2}$ following excitation of $^4G_{7/2}$ and subsequent nonradiative decay. Excitation wavelengths are 293.2 nm (Er:YAG), 293.0 nm (Tm,Er:YSAG), and 293.4 nm (Cr,Er:YSGG).

ly much smaller than the total number of G^K_{iQ} parameters contained in $\hat{H}_{\text{occf}}$. For more detailed discussion of the $\hat{H}_{\text{occf}}$ Hamiltonian and its use in crystal-field energy-level analyses, the reader is referred to Refs. 30, 32, 44, and 45.

The energy-level analyses performed in this study were based on a strategy that included three main steps in fitting calculated levels to experimental energy-level data. In the *first step,* the parameters of the atomic Hamiltonian $\hat{H}_a$ were adjusted to yield optimum fits between calculated and experimentally determined J-multiplet barycenter energies. In the *second step,* parameters of both the atomic Hamiltonian $\hat{H}_a$ *and* the one-electron crystal-field Hamiltonian $\hat{H}_{\text{cf}}$ were varied to obtain optimized fits between calculated and experimentally determined crystal-field energy-level data. In the *third step,* specific parts of the correlation crystal-field Hamiltonian $\hat{H}_{\text{occf}}$ were incorporated into the analyses for the purpose of resolving major discrepancies between calculated and observed crystal-field splittings within certain J-multiplet energy-level manifolds. Each step involved many iterative calculations in which various parts of the relevant parameter surfaces were explored, and the final data fits also reflect iterative calculations over all three steps.

Among the 20 parameters associated with the atomic Hamiltonian, 16 were treated as independent fitting variables. Four of the atomic parameters, M^2, M^4, P^4, and P^6, were constrained according to $M^2=0.56M^0$, $M^4=0.38M^0$, $P^4=0.75P^2$, and $P^6=0.50P^2$. In performing data fits all nine B^k_q parameters in the one-electron crystal-field Hamiltonian were treated as independent variables. The experimental data sets include 117 Stark levels spanning 29 J multiplets and 12 LS terms for Er^{3+} in YAG, 109 Stark levels spanning 29 J multiplets and 12 LS terms for Er^{3+} in YSAG, and 92 Stark levels spanning 22 J multiplets and 9 LS terms for Er^{3+} in YSGG.

Energy-level analyses based on the $(\hat{H}_a+\hat{H}_{\text{cf}})$ Hamiltonian gave particularly large discrepancies between calculated and observed crystal-field splittings within the $^2H(2)_{11/2}$ multiplet manifold (centered at about 19 240 cm^{-1}) and the $^2H(2)_{9/2}$ multiplet manifold (centered at about 36 530 cm^{-1}). These discrepancies could not be improved by any combination of adjustments in the one-electron crystal-field interaction parameters (B^k_q) without causing serious degradation in the quality of the *overall* data fits. Therefore, the crystal-field energy-level structures within the $^2H(2)_{11/2}$ and $^2H(2)_{9/2}$ multiplets were targeted for *correlation crystal-field* (CCF) analysis. Among the many terms in the $\hat{H}_{\text{occf}}$ Hamiltonian [defined according to Eq. (4)], only a few with $i>1$ have large matrix elements *within* the $^2H(2)_{11/2}$ and $^2H(2)_{9/2}$ state manifolds, and we restricted our CCF analysis to these terms. Extensive computational explorations revealed that just one of these terms (with $K=4$ and $i=10A$) is needed to give dramatic improvements in the agreement between calculated and observed crystal-field splittings within the targeted multiplet manifolds, while leaving the already well-fitted, nonproblematic multiplet manifolds relatively unaffected.

The actual Hamiltonian used in the final CCF energy-level calculations was

$$\hat{H}=\hat{H}_a+\hat{H}_{\text{cf}}+G^4_{10A}[\hat{g}^{(4)}_{10A0}+(B^4_2/B^4_0)\hat{g}^{(4)}_{10A2}+(B^4_4/B^4_0)\hat{g}^{(4)}_{10A4}] \quad (5)$$

where $\hat{H}_a$ is defined according to Eq. (2), $\hat{H}_{\text{cf}}$ is given by Eq. (3b), and it is assumed that the Q dependence of the CCF parameters is given by[30]

$$G^4_{10AQ}=G^4_{10A}(B^4_q/B^4_0)\ , \quad (6)$$

where $G^4_{10A}=G^4_{10A0}$. Given the assumption underlying Eq. (6), only one parameter is needed to represent the CCF contributions to the model Hamiltonian shown in Eq. (5). It is interesting to point out that model Hamiltonians of identical (or similar) form have been used with success in the analysis of the crystal-field energy-level structures of Nd^{3+} in a variety of host materials.[30–32]

Most of the calculated results reported in this paper were obtained from calculations and analyses based on the methods and strategies described above. An important objective of those calculations and analyses was to characterize and compare both the *atomic* and *crystal-field* interaction parameters in the model Hamiltonians for the respective Er^{3+}:garnet systems. This was done by using 16 atomic parameters and either nine or ten crystal-field parameters as independent variables in performing fits of calculated-to-experimental energy-level data. The empirical data sets used in these fits were adequate for supporting the 25- (or 26) parameter analyses.

To help establish the data sets, a separate series of calculations was performed that focused solely on the *one-electron crystal-field* parametrization of the model Hamiltonian. The latter analyses were carried out according to procedures used with great success by Morrison and Leavitt in their extensive studies of $4f^N$ electronic energy-level structures in Ln^{3+}-doped systems.[25] Intermediate-coupling f^{11} $[SL]J$ wave functions were calculated using the atomic Hamiltonian (and parameters) reported by Carnall, Fields, and Rajnak[46] for Er^{3+} (aquo) ions, and these wave functions were then used as basis functions in the crystal-field energy-level calculations. Calculated-versus-experimental data fits were performed by treating the nine B^k_q crystal-field parameters of $\hat{H}_{\text{cf}}$ [see Eq. (3b)] as free variables, while *also* permitting the centroids of the $[SL]J$ multiplets to vary freely. In these calculations, "interactions" (or covariances) between atomic and crystal-field Hamiltonian parameters are avoided, and the crystal-field Hamiltonian should be entirely free of any burdens associated with multiplet barycenter adjustments. Because the barycenters are independently adjustable, we can evaluate the experimental data for each multiplet independently. This program has been valuable in choosing levels for a final evaluation in the extended calculation. However, we need to keep in mind that the $[SL]J$ basis functions used in these calculations are derived from a very approximate atomic Hamiltonian, and it is possible that inaccuracies in the $[SL]J$ basis set will distort the crystal-field parametrization results.

IV. RESULTS

The atomic and crystal-field Hamiltonian parameters derived from our energy-level analyses are listed in Table

I. Two sets of parameter values are listed for each of the three Er^{3+}:garnet systems examined in this study. One set was obtained from analyses in which CCF terms were *excluded* from the crystal-field Hamiltonian, and the other set was obtained from analyses in which the CCF terms shown in Eq. (5) were included. Recall from our earlier discussion that although the Hamiltonian defined by Eq. (5) contains three CCF operators, $\hat{g}^{(4)}_{10AQ}$ ($Q=0$, 2, and 4), only one of the three corresponding CCF parameters was treated as a free variable in our calculated-to-experimental energy-level fits. The remaining two parameters were constrained according to Eq. (6). The G^4_{10A} parameter listed in Table I corresponds to G^4_{10A0}. Values for the G^4_{10A2} and G^4_{10A4} parameters may be calculated by substitution of the appropriate values of G^4_{10A}, B^4_0, B^4_2, and B^4_4 (from Table I) into Eq. (6). The CCF operators in Eq. (5) have normalization properties that differ from the normalization properties of the one-electron crystal-field operators (contained in $\hat{H}_{cf}$).[30,32] However, the G^4_{10AQ}/B^4_q parameter ratios obtained for the three systems examined in this study are of some interest for comparative purposes. These ratios are -0.39 (for Er^{3+}:YAG), -0.30 (for Er^{3+}:YSAG), and -0.22 (for Er^{3+}:YSGG). These values for G^4_{10AQ}/B^4_q may be compared to the values -0.56 (for Nd^{3+}:YAG) and -0.28 (for $NdAlO_3$) reported by Li and Reid.[30]

Calculated and experimentally observed energy-level

TABLE I. Hamiltonian parameters derived from parametric fits of calculated-to-experimental energy-level data. All parameter values are expressed in units of cm^{-1}.

	Er^{3+}:YAG[b]		Er^{3+}:YSAG[b]		Er^{3+}:YSGG[b]	
Parameter[a]	(No CCF)[c]	(CCF)[d]	(No CCF)[c]	(CCF)[d]	(No CCF)[c]	(CCF)[d]
E_{av}	35 660	35 656	35 681	35 672	35 680	35 684
F^2	99 394	99 333	99 522	99 394	99 443	99 450
F^4	70 394	70 581	71 417	71 415	70 775	70 774
F^6	48 908	49 207	50 232	50 288	49 508	49 397
α	17.4	17.6	17.7	17.9	18.8	19.2
β	−605	−612	−625	−632	−646	−645
γ	1 780	1 698	1 421	1 416	1 691	1 708
T^2	640	599	554	515	[546][g]	[546][g]
T^3	40.3	37.6	40.1	37.3	40.4	38.9
T^4	73.5	69.4	83.7	80.5	[88][g]	[88][g]
T^6	−369	−362	−361	−366	−349	−347
T^7	330	323	280	271	359	367
T^8	564	505	584	551	415	349
ζ	2 368.9	2 368.4	2 370.0	2 368.8	2 365.5	2 363.6
M^0	3.6	3.6	3.6	3.5	3.7	3.6
P^2	501	478	517	477	458	418
B^2_0	−455	−446	−412	−435	−434	−502
B^2_2	−319	−310	−383	−365	−135	−118
B^4_0	−155	−224	−193	−272	−225	−108
B^4_2	−1 797	−1 794	−1 725	−1 742	−1 716	−1 680
B^4_4	−581	−507	−954	−880	−954	−878
B^6_0	1 501	1 487	1 506	1 440	1 185	1 026
B^6_2	327	361	276	394	326	417
B^6_4	−618	−634	−466	−494	−560	−541
B^6_6	569	514	506	453	501	666
G^4_{10A}		85.8[h]		81.3[h]		23.9[h]
σ[e]	16.40	13.20	15.74	13.59	13.54	11.95
N[f]	117	117	109	109	92	92

[a]Parameters are defined and labeled according to Eqs. (2), (3), and (5) in the text.

[b]Er^{3+}:YAG$\equiv Er^{3+}:Y_3Al_5O_{12}$; Er^{3+}:YSAG$\equiv Tm^{3+},Er^{3+}:Y_3Sc_2Al_3O_{12}$; and Er^{3+}:YSGG $\equiv Cr^{3+},Er^{3+}:Y_3Sc_2Ga_3O_{12}$. See text for a description of the compositions of these systems.

[c]Parameter values obtained from analysis in which *No CCF* terms were included in the model Hamiltonian.

[d]Parameter values obtained from analyses in which the CCF terms shown in Eq. (5) were included in the model Hamiltonian.

[e]rms deviation between calculated and experimental energies.

[f]Number of experimental levels included in the data fits.

[g]These parameter values were held fixed in the final calculation.

[h]The G^4_{10A} parameter corresponds to the CCF parameter G^4_{10A0} [see eq. (5)]. Values for the G^4_{10A2} and G^4_{10A4} CCF parameters may be obtained from the relations expressed in Eq. (6) of the text.

TABLE II. Calculated and experimental energy levels. All energies are expressed in units of cm^{-1}.

Level number	Multiplet label[a]	Er^{3+}:YAG[b]			Er^{3+}:YSAG[b]			Er^{3+}:YSGG[b]		
		Calc.[c]	Expt.[d]	Δ[e]	Calc.[c]	Expt.[d]	Δ[e]	Calc.[c]	Expt.[d]	Δ[e]
1	$^4I_{15/2}$	−31	0[f]	−31	−18	0[g]	−18	−9	0[h]	−9
2	$^4I_{15/2}$	1	22[f]	−21	1	21[g]	−20	14	33[h]	−19
3	$^4I_{15/2}$	40	60[f]	−20	35	60[g]	−25	29	41[h]	−11
4	$^4I_{15/2}$	76	80[f]	−4	78	86[g]	−8	57	71[h]	−14
5	$^4I_{15/2}$	388	417[f]	−29	394	385[g]	9	389	380[h]	−9
6	$^4I_{15/2}$	430	432[f]	−2	425	418[g]	7	411	410[h]	1
7	$^4I_{15/2}$	498			487			479	485[h]	−6
8	$^4I_{15/2}$	575	574[f]	1	553	555[g]	−2	502	503[h]	−1
9	$^4I_{13/2}$	6 558	6 549[f]	9	6 543	6 544	−1	6 553	6 557	−4
10	$^4I_{13/2}$	6 610	6 599[f]	11	6 613	6 600	13	6 588	6 580	8
11	$^4I_{13/2}$	6 621	6 606[f]	15	6 619	(6 606)[i]		6 603	6 594	9
12	$^4I_{13/2}$	6 786	6 786[f]	0	6 791	6 774	17	6 783	6 784	−1
13	$^4I_{13/2}$	6 837	6 805[f]	32	6 829	6 797	32	6 798	6 793	5
14	$^4I_{13/2}$	6 886	6 883[f]	3	6 879	6 873	6	6 862	6 844	18
15	$^4I_{13/2}$	6 904	6 889[f]	15	6 894	6 889	5	6 872	6 854	−18
16	$^4I_{11/2}$	10 255	10 255[f]	0	10 249	10 252	−3	10 244	10 256	−12
17	$^4I_{11/2}$	10 290	10 285[f]	5	10 292	10 287	5	10 270	10 272	−2
18	$^4I_{11/2}$	10 359	10 361[f]	−2	10 363	10 367	−4	10 349	10 353	−4
19	$^4I_{11/2}$	10 382	10 372[f]	10	10 384	(10 358)[i]		10 361	10 361	0
20	$^4I_{11/2}$	10 413	10 412[f]	1	10 409	10 416	−7	10 394	10 392	2
21	$^4I_{11/2}$	10 422	10 417[f]	5	10 417	10 423	−6	10 403	10 395	8
22	$^4I_{9/2}$	12 282	12 297[f]	−15	12 291	12 308	−17	12 296	12 312	−16
23	$^4I_{9/2}$	12 503	12 522[f]	−19	12 505	12 525	−20	12 534	12 547	−13
24	$^4I_{9/2}$	12 550	12 572[f]	−22	12 567	12 567	0	12 564	12 574	−10
25	$^4I_{9/2}$	12 702	12 714[f]	−12	12 676	12 688	−12	12 669	12 694	−25
26	$^4I_{9/2}$	12 748	12 759[f]	−9	12 747	12 760	−13	12 734	12 739	−5
27	$^4F_{9/2}$	15 303	15 288	15	15 302	15 287	15	15 310	15 297	13
28	$^4F_{9/2}$	15 334	15 312	22	15 327	15 315	12	15 339	15 321	18
29	$^4F_{9/2}$	15 385	15 357	28	15 381	15 369	11	15 371	15 345	26
30	$^4F_{9/2}$	15 484	15 473	11	15 471	15 470	1	15 477	15 464	13
31	$^4F_{9/2}$	15 515	15 518	−3	15 533	15 525	8	15 527	15 502	25
32	$^4S_{3/2}$	18 399	18 394	5	18 397	18 398	−1	18 407	18 411	−4
33	$^4S_{3/2}$	18 458	18 459	−1	18 472	18 471	1	18 461	18 454	7
34	$^2H(2)_{11/2}$	19 120	19 094	26	19 125	19 107	18	19 117	19 106	11
35	$^2H(2)_{11/2}$	19 140	19 114	26	19 140	19 126	14	19 135	19 122	13
36	$^2H(2)_{11/2}$	19 171	19 152	19	19 181	19 155	26	19 166	19 154	12
37	$^2H(2)_{11/2}$	19 355	19 348	7	19 361	19 350	11	19 337	19 340	−3
38	$^2H(2)_{11/2}$	19 367	19 366	1	19 386	19 368	18	19 359	19 356	3
39	$^2H(2)_{11/2}$	19 379	19 370	9	19 400			19 367	19 360	7
40	$^4F_{7/2}$	20 512	20 514	−2	20 517	20 515	2	20 508	20 530	−22
41	$^4F_{7/2}$	20 549	20 570	−21	20 553	20 578	−25	20 566	20 576	−10
42	$^4F_{7/2}$	20 649	20 650	−1	20 642	20 652	−10	20 639	20 645	−6
43	$^4F_{7/2}$	20 697	20 701	−4	20 707	20 714	−7	20 682	20 685	−3
44	$^4F_{5/2}$	22 224	22 224	0	22 227	22 224	3	22 229	22 224	5
45	$^4F_{5/2}$	22 244	22 244	0	22 245	22 241	4	22 233		
46	$^4F_{5/2}$	22 289	22 291	−2	22 294	22 294	0	22 280	22 285	−5
47	$^4F_{3/2}$	22 607	22 595	12	22 625	22 587	38	22 598	22 609	−11
48	$^4F_{3/2}$	22 657	22 666	−9	22 667	22 672	−5	22 647	22 649	−2
49	$^2G_{9/2}$	24 416	24 423	−7	24 425	24 427	−2	24 432	24 436	−4

TABLE II (*Continued*)

Level number	Multiplet label[a]	Er^{3+}:YAG[b] Calc.[c]	Er^{3+}:YAG[b] Expt.[d]	Er^{3+}:YAG[b] Δ[e]	Er^{3+}:YSAG[b] Calc.[c]	Er^{3+}:YSAG[b] Expt.[d]	Er^{3+}:YSAG[b] Δ[e]	Er^{3+}:YSGG[b] Calc.[c]	Er^{3+}:YSGG[b] Expt.[d]	Er^{3+}:YSGG[b] Δ[e]
50	$^2G_{9/2}$	24 581	24 577	4	24 582	24 575	7	24 607	24 581	26
51	$^2G_{9/2}$	24 605	24 593	12	24 619	24 608	11	24 621	24 604	17
52	$^2G_{9/2}$	24 752	24 765	−13	24 733	24 760	−27	24 732	24 751	−19
53	$^2G_{9/2}$	24 781	24 785	−4	24 780	24 787	−7	24 775	24 772	3
54	$^4G_{11/2}$	26 233	26 215	18	26 240	26 232	8	26 239	26 241	−2
55	$^4G_{11/2}$	26 273	26 277	−4	26 284	26 292	−8	26 274	26 287	−13
56	$^4G_{11/2}$	26 322	26 323	−1	26 317	26 328	−11	26 312	26 332	−20
57	$^4G_{11/2}$	26 564	26 567	−3	26 570	26 574	−4	26 554	26 564	−10
58	$^4G_{11/2}$	26 573	26 574	−1	26 582	26 574	8	26 575	26 575	0
59	$^4G_{11/2}$	26 609	26 605	4	26 622	26 609	13	26 601	26 602	−1
60	$^2K_{15/2}$	27 293	27 298	−5	27 267			27 297		
61	$^4G_{9/2}$	27 325	27 322	3	27 318	27 309	9	27 314	27 321	−7
62	$^2K_{15/2}$	27 348	27 368	−20	27 319	27 334	−15	27 366	27 339	−27
63	$^4G_{9/2}$	27 481	27 486	−5	27 479	27 493	−14	27 473	(27 427)[i]	
64	$^4G_{9/2}$	27 493	27 498	−5	27 495	27 507	−12	27 491	27 487	4
65	$^4G_{9/2}$	27 520	27 531	−11	27 521	27 539	−18	27 512	27 502	10
66	$^2K_{15/2}$	27 586	27 585	1	27 614	27 601	13	27 573	27 552	21
67	$^2K_{15/2}$	27 605	27 596	9	27 634	27 637	−3	27 589	27 578	11
68	$^2K_{15/2}$	27 737			27 793	(27 824)[i]		27 816	27 820	−4
69	$^2K_{15/2}$	27 857			27 901	27 885	16	27 872	27 875	−3
70	$^2K_{15/2}$	27 921	27 920	1	27 969	27 975	−6	27 933		
71	$^2K_{15/2}$	28 005	27 980	25	28 058	28 074	−16	28 070	28 062	8
72	$^4G_{9/2}$	28 047			28 079	28 090	−11	28 085	28 080	5
73	$^2G_{7/2}$	28 081	28 070	11	28 105	28 108	−3	28 103	28 113	−10
74	$^2G_{7/2}$	28 121	28 117	4	28 129	28 121	8	28 126	28 137	−11
75	$^2G_{7/2}$	28 146	28 150	−4	28 151	28 145	6	28 152	28 147	5
76	$^2G_{7/2}$	28 153	28 166	−13	28 160	28 167	−7	28 156		
77	$^2P_{3/2}$	31 506	31 480	26	31 505	31 485	20	31 515	31 516	−1
78	$^2P_{3/2}$	31 596	31 600	−4	31 601	31 614	−13	31 592	31 585	7
79	$^2K_{13/2}$	32 594			32 585			32 647		
80	$^2K_{13/2}$	32 817	32 814	3	32 854	32 840	14	32 806	32 815	−9
81	$^2K_{13/2}$	32 833	32 855	−22	32 870			32 839	32 855	−16
82	$^2K_{13/2}$	32 983			33 010	(33 015)[i]		33 026		
83	$^2P_{1/2}$	33 016	33 026	−10	33 033	33 037	−4	33 046	33 060	−14
84	$^4G_{5/2}$	33 076	33 085	−9	33 074	33 096	−22	33 078	33 070	8
85	$^2K_{13/2}$	33 162	33 166	−4	33 178	33 179	−1	33 134	33 126	8
86	$^2K_{13/2}$	33 226	33 246	−20	33 262	(33 260)[i]		33 246	33 263	−17
87	$^2K_{13/2}$	33 303	(33 301)[i]		33 330	33 357	−27	33 332		
88	$^4G_{5/2}$	33 353	33 338	15	33 388	33 381	7	33 380	33 376	4
89	$^4G_{5/2}$	33 476	(33 469)[i]		33 468	33 441	27	33 443	33 450	−7
90	$^4G_{7/2}$	33 996	34 014	−18	34 001	(34 015)[i]		34 022	34 023	−1
91	$^4G_{7/2}$	34 034	34 030	4	34 040	34 038	2	34 045	34 055	−10
92	$^4G_{7/2}$	34 052	34 097	45	34 060	34 089	−29	34 078	34 085	−7
93	$^4G_{7/2}$	34 190	34 172	18	34 180	34 166	14	34 167	34 157	10
94	$^2D(1)_{5/2}$	34 734			34 733			34 754	34 773	−19
95	$^2D(1)_{5/2}$	34 786	34 792	−6	34 780	34 797	−17	34 789	34 790	−1
96	$^2D(1)_{5/2}$	34 893	34 897	−4	34 898	34 905	−7	34 895	34 880	15
97	$^2H(2)_{9/2}$	36 348	36 332	16	36 355	36 336	19	36 359	36 351	8
98	$^2H(2)_{9/2}$	36 416	36 400	16	36 449			36 432	36 409	23
99	$^2H(2)_{9/2}$	36 498	36 504	−6	36 501	36 499	2	36 504	(36 499)[i]	
100	$^2H(2)_{9/2}$	36 578	36 586	−8	36 586	36 587	−1	36 554	36 567	−13
101	$^2H(2)_{9/2}$	36 816	36 813	3	36 806	36 804	2	36 767	36 782	−15

TABLE II (*Continued*)

Level number	Multiplet label[a]	Er^{3+}:YAG[b] Calc.[c]	Er^{3+}:YAG[b] Expt.[d]	Δ[e]	Er^{3+}:YSAG[b] Calc.[c]	Er^{3+}:YSAG[b] Expt.[d]	Δ[e]	Er^{3+}:YSGG[b] Calc.[c]	Er^{3+}:YSGG[b] Expt.[d]	Δ[e]
102	$^4D_{5/2}$	38 509	38 500	9	38 505	38 492	13	38 559		
103	$^4D_{5/2}$	38 550	38 535	15	38 538	38 521	17	38 594		
104	$^4D_{5/2}$	38 568	38 570	−2	38 559	38 576	−17	38 628		
105	$^4D_{7/2}$	39 035	39 020	15	39 067	39 071	−4	39 105		
106	$^4D_{7/2}$	39 067	39 065	2	39 087			39 159		
107	$^4D_{7/2}$	39 192			39 242	(39 179)[i]		39 233		
108	$^4D_{7/2}$	39 344	39 360	−16	39 384	(39 395)[i]		39 384		
109	$^2I_{11/2}$	40 878	40 871	7	40 893	40 870	23	40 972		
110	$^2I_{11/2}$	40 948	40 938	10	40 943	40 948	−5	41 028		
111	$^2I_{11/2}$	40 970	40 968	2	40 971	40 966	5	41 047		
112	$^2I_{11/2}$	41 011	41 006	5	41 011	41 002	9	41 080		
113	$^2L_{17/2}$	41 102			41 089			41 168		
114	$^2I_{11/2}$	41 137	41 138	−1	41 126	41 120	6	41 215		
115	$^2I_{11/2}$	41 199	41 206	−7	41 181	41 194	−13	41 365		
116	$^2L_{17/2}$	41 330	41 318	12	41 326	41 310	16	41 515		
117	$^2L_{17/2}$	41 421			41 422	(41 428)[i]		41 549		
118	$^2L_{17/2}$	41 487	41 500	−13	41 481	41 481	0	41 616		
119	$^2L_{17/2}$	41 514			41 516	(41 516)[i]		41 622		
120	$^2L_{17/2}$	41 558	41 546	12	41 566	41 550	16	41 666		
121	$^2L_{17/2}$	41 583	41 571	12	41 580			41 687		
122	$^2L_{17/2}$	41 616	41 622	−6	41 617	41 637	−20	41 759		
123	$^2L_{17/2}$	41 732	41 730	2	41 716	41 706	10	41 902		
124	$^4D_{3/2}$	42 198	42 208	−10	42 212	42 210	2	42 219		
125	$^4D_{3/2}$	42 245	42 260	−15	42 263	42 270	−7	42 261		
126	$^2P_{3/2}$	42 750	42 759	−9	42 724			42 795		
127	$^2P_{3/2}$	42 803	42 804	−1	42 784			42 842		
128	$^2I_{13/2}$	43 314	43 310	4	43 311	43 307	4	43 376		
129	$^2I_{13/2}$	43 346			43 350	43 371	−21	43 422		
130	$^2I_{13/2}$	43 399	43 414	−15	43 407	43 420	−13	43 465		
131	$^2I_{13/2}$	43 452	43 465	−13	43 454	43 469	−15	43 492		
132	$^2I_{13/2}$	43 648	(43 655)[i]		43 659			43 724		
133	$^2I_{13/2}$	43 710			43 746	(43 731)[i]		43 770		
134	$^2I_{13/2}$	43 860			43 895			43 899		

[a]Multiplet label reflects principal *SLJ* parentage of the calculated level.
[b]See footnote b of Table I.
[c]From calculations based on the model Hamiltonian given by Eq. (5) in the text, with atomic and crystal-field parameter values as listed in Table I.
[d]Particulars regarding the sources of experimental data are given in the text.
[e]Difference between calculated and experimental energies (in cm^{-1}).
[f]Emission data from $^4S_{3/2}\rightarrow{}^4I_{15/2}$ and $^2P_{3/2}\rightarrow{}^4I_{13/2}$, $^4I_{11/2}$, and $^4I_{9/2}$.
[g]Emission data from lowest $^4S_{3/2}$ excited level.
[h]Emission data from $^4S_{3/2}\rightarrow{}^4I_{15/2}$.
[i]Energy levels in parentheses were not used in the fitting calculations.

data are listed in Table II for each of the Er^{3+}:garnet systems examined in this study. The calculated energies shown in Table II were obtained as eigenvalues of the Hamiltonian defined by Eq. (5), with atomic and crystal-field parameter values as listed in Table I for the respective systems. Energy-level data calculated *without* the inclusion of CCF terms in the crystal-field Hamiltonian are not given in Table II, but comparisons of *crystal-field splitting energies* calculated *with* and *without* the inclusion of CCF terms are shown in Table III. As we stated earlier (in Sec. III), reasonable agreement between calculated and observed crystal-field splittings within the $^2H(2)_{11/2}$ and $^2H(2)_{9/2}$ multiplet manifolds can be achieved *only* when the $\hat{g}^{(4)}_{10AQ}$ CCF operators are includ-

TABLE III. Comparisons between calculated and experimental crystal-field splittings within the $^2H(2)_{11/2}$, $^2H(2)_{9/2}$, $^4I_{11/2}$, and $^4G_{11/2}$ multiplet manifolds. All energies are expressed in units of cm^{-1}.

Level number[a]	Er^{3+}:YAG $\tilde{\nu}$[b]	Expt.[c]	CCF[d]	No CCF[e]	Er^{3+}:YSAG $\tilde{\nu}$[b]	Expt.[c]	CCF[d]	No CCF[e]	Er^{3+}:YSGG $\tilde{\nu}$[b]	Expt.[c]	CCF[d]	No CCF[e]
					$^2H(2)_{11/2}$							
34	19 094	−147	−135	−109	19 107		−141	−121	19 106	−134	−130	−113
35	19 114	−127	−115	−92	19 126		−126	−105	19 122	−118	−112	−101
36	19 152	−89	−84	−68	19 155		−85	−65	19 154	−86	−81	−73
37	19 348	107	100	80	19 350		95	83	19 340	100	90	81
38	19 366	125	112	91	19 368		120	97	19 356	116	112	96
39	19 370	129	124	96			134	109	19 360	120	120	109
σ[f]			9.6	31.8							5.7	17.2
Baricenter		19 241	19 255	19 253		h	19 266	19 261		19 240	19 247	19 249
σ[g]			17.5	34.0			16.5	27.2			9.1	19.5
					$^2H(2)_{9/2}$							
97	36 332	−195	−183	−185	36 336		−184	−185	36 351	−171	−164	−158
98	36 400	−127	−115	−120			−90	−101	36 409	−113	−91	−97
99	36 504	−23	−33	−1	36 499		−38	−10	(36 499)[i]	−23	−19	−1
100	36 586	59	47	67	36 587		47	67	36 567	45	31	39
101	36 813	286	285	240	36 804		267	228	36 782	260	244	215
σ[f]			10.3	23.7							14.1	24.3
Baricenter		36 527	36 531	36 529		h	36 539	36 537		36 522	36 523	36 527
σ[g]			11.1	23.8			9.6	26.7			15.7	24.3
					$^4I_{11/2}$							
16	10 255	−95	−99	−111	10 252	−99	−103	−113	10 256	−82	−93	−100
17	10 285	−65	−64	−73	10 287	−64	−60	−67	10 272	−66	−67	−72
18	10 361	11	5	7	(10 358)[i]	7	11	12	10 353	15	12	9
19	10 372	22	28	39	10 367	16	32	43	10 361	23	24	31
20	10 412	62	59	66	10 416	65	57	59	10 392	54	57	65
21	10 417	67	68	72	10 423	72	65	68	10 395	57	66	68
σ[f]			4.1	10.5			8.3	13.0			8.5	13.2
Baricenter		10 350	10 354	10 354		10 351	10 352	10 353		10 338	10 337	10 338
σ[g]			5.1	11.2			8.5	13.2			6.2	10.8
					$^4G_{11/2}$							
54	26 215	−212	−196	−178	26 232	−203	−196	−181	26 241	−193	−187	−180
55	26 277	−150	−156	−139	26 292	−143	−152	−140	26 287	−147	−152	−146
56	26 323	−104	−107	−105	26 328	−107	−119	−112	26 332	−102	−114	−111
57	26 567	140	135	124	26 574	139	134	126	26 564	130	128	124
58	26 574	147	144	128	26 574	139	146	133	26 575	141	149	142
59	26 605	178	180	169	26 609	174	186	176	26 602	168	175	173
σ[f]			7.5	18.1			9.1	11.0			7.3	7.2
Baricenter		26 427	26 429	26 430		26 435	26 436	26 434		26 434	26 426	26 426
σ[g]			7.8	18.4			9.1	11.0			10.6	10.1

[a]Level numbering corresponds to that used in Table II.
[b]Experimentally determined energy (in cm^{-1}).
[c]Splitting energy measured from multiplet baricenter (from experiment).
[d]Splitting energy measured from multiplet baricenter (from calculations that included CCF terms in the model Hamiltonian).
[e]Splitting energy measured from multiplet baricenter (from calculations that did NOT include CCF terms in the model Hamiltonian).
[f]The rms deviation between calculated and observed crystal-field splitting energies in cm^{-1}.
[g]The rms deviation between calculated and observed crystal-field energies (with no dependence on the baricenter location).
[h]Experimental baricenter was not determinable, since at least one crystal-field level was unassigned.
[i]Energy levels in parentheses were not used in fitting calculations to determine atomic and crystal-field parameters.

ed in the model Hamiltonian. From the results given in Table III, we see that inclusion of these operators also improves agreement between calculated and observed crystal-field splittings within the $^4I_{11/2}$ and $^4G_{11/2}$ multiplet manifolds.

The B_q^k parameter values listed in Table I (in the *No CCF* columns) are essentially identical to those obtained from analyses in which the atomic Hamiltonian was assigned a set of "fixed" parameters, and the experimental energy-level data were fitted by J-multiplet baricenter energies and the B_q^k crystal-field parameters being treated as free variables. The latter analyses produced calculated-to-experimental data fits with rms deviations of 14.4 cm^{-1} (Er^{3+}:YAG), 13.4 cm^{-1} (Er^{3+}:YSAG), and 11.7 cm^{-1} (Er^{3+}:YSGG), which are comparable to those given in Table I.

We note from Table II that the crystal-field splittings calculated for the $^4I_{15/2}$ *(ground)* multiplet are in relatively poor agreement with experimental observation. Considerable effort was devoted to resolving this problem, but without much success. Among the terms in the CCF Hamiltonian, those with $\hat{g}_{3Q}^{(6)}$ operators have the largest matrix elements within the $^4I_{15/2}$ state manifold. However, inclusion of these terms in the Hamiltonian did not produce significantly better agreement between calculated and experimental energy levels. Adjustments of the one-electron crystal-field parameters (B_q^k) to optimize calculated-versus-observed energy-level fits within the $^4I_{15/2}$ multiplet invariably caused serious problems in other parts of the overall energy-level structures (for the respective Er^{3+}:garnet systems). Specifically, the levels of the mixed multiplets ($^4G_{9/2}$, $^2K_{15/2}$) and ($^2I_{11/2}$, $^2L_{17/2}$) are affected if a set of crystal-field parameters that more accurately reflects the ground state is used. In the program with variable multiplet baricenters, the baricenters of the $^4G_{9/2}$ and $^2K_{15/2}$ can be shifted relative to one another and still match all the experimental data with overall rms deviations comparable to those given above (this changes the major parentage of some of the levels in these multiplets). However, this was not possible in the ($^2I_{11/2}$, $^2L_{17/2}$) multiplets with all of the data given in Table II. A substantial improvement in the fits for both Er^{3+}:YAG and Er^{3+}:YSAG is possible by deleting the levels in the $^2L_{17/2}$ multiplet from the calculation. Further evaluation of the levels in the $^2L_{17/2}$ multiplet may lead to further refinement of the parameters. However, for the data sets as given in Table II, these are the optimal fits.

In general, the atomic Hamiltonian parameters shown in Table I have very similar values for the Er^{3+}:YAG, Er^{3+}:YSAG, and Er^{3+}:YSSG systems. Furthermore, these parameter values are also very similar to those reported previously for another system in which Er^{3+} ions are also coordinated to negatively charged oxygen atoms, $Na_3[Er(C_4H_4O_5)_3]\cdot 2NaClO_4\cdot 6H_2O$.[47] A major-component analysis of the $4f^{11}$ $[SL]J$ state vectors calculated for the various Er^{3+}:garnet systems is not presented here. Instead, the reader is referred to Table IV of Ref. 47, in which a major-component analysis is presented for the $4f^{11}$ $[SL]J$ state vectors of Er^{3+} in $Na_3[Er(C_4H_4O_5)_3]\cdot 2NaClO_4\cdot 6H_2O$ (which are very similar to those calculated for the Er^{3+}:garnet systems examined in the present study).

The signs of the crystal-field parameters, B_q^k, calculated for the Er^{3+}:YAG, Er^{3+}:YSAG, and Er^{3+}:YSGG systems are the same for a given k and q (see Table I), the magnitudes of the B_0^2 parameters are reasonably similar for the three systems, and in each case the B_2^4 parameter has the largest magnitude and the B_0^6 parameter has the next-to-the-largest magnitude. The relative orderings of the remaining B_q^k parameters (with respect to magnitude) show some significant variations among the three Er^{3+}:garnet systems. The strongest distinctions between systems are reflected in the B_2^2 parameter values (compare Er^{3+}:YSGG to Er^{3+}:YSAG and Er^{3+}:YAG), and in the B_4^4 parameter values (compare Er^{3+}:YAG to Er^{3+}:YSAG and Er^{3+}:YSGG). We also note that the CCF parameter G_{10A}^4 has a significantly smaller value for Er^{3+}:YSGG than for either Er^{3+}:YAG or Er^{3+}:YSAG.

The electrostatic crystal-field interactions are noticeably sensitive to any change in the coordination sphere surrounding the Er^{3+} ions. This sensitivity depends on the distance between the Er^{3+} ions and the oxygen ions that make up the coordination sphere. Based on crystallographic studies that determined distances between ions in the unit cell,[40] the anticipated ordering of $|B_q^k|$ (for a given k,q) is YAG > YSAG > YSGG. This predicted trend of $|B_q^k|$ parameters agrees with the final set of parameters obtained from the analysis of the spectroscopic data for B_0^2 [except for YSGG (CCF)], B_2^4, B_0^6, B_2^6] [except for YSGG (CCF)], B_4^6, and B_6^6. The relatively large value of G_{10A}^4 for Er^{3+}:YAG may rationalize the unusually low value of B_4^4 for that garnet. Since $\hat{U}_4^4$ and $\hat{g}_{10A}^4$ have the same rank, the former could have been affected by the inclusion of the second-order operators. The rank-six crystal-field parameters are most likely to reflect differences in Er-O distances (and hence the crystal-field splitting), because rank-six operators are most sensitive to the electrostatic interactions between the erbium ion and the first coordination sphere. The dependence of the electric-field strength with ionic distance is also shown by the trend in G_{10A}^4. The experimental multiplet manifold splittings for $^2H(2)_{11/2}$ and $^2H(2)_{9/2}$ are slightly larger in Er^{3+}:YAG than in the other garnets. The value of G_{10A}^4 for Er^{3+}:YAG (Table I) is larger than G_{10A}^4 for Er^{3+}:YSAG and Er^{3+}:YSGG.

V. DISCUSSION AND CONCLUSIONS

In this paper we have reported data and analyses of $4f^{11}$ electronic energy-level structures in three Er^{3+}-doped garnet systems. The energy-level analyses were based on the use of a parametrized model Hamiltonian that assumes D_2 site symmetry for the Er^{3+} ions. The parameters of this model Hamiltonian were treated as variables in performing fits of calculated-to-experimental energy-level data for each of the three Er^{3+}:garnet systems, and differences between the "optimized" parameter values obtained from the respective data fits may be correlated with differences between crystal-field interac-

tion details in the three systems.

The atomic Hamiltonian parameters characterized from our energy-level analyses have generally similar values for the Er^{3+}:YAG, Tm^{3+}, Er^{3+}:YSAG, and Cr^{3+}, Er^{3+}:YSGG systems. This suggests that the *isotropic* parts of the $4f$-electron crystal-field interactions are similar in these systems, which is not surprising. On the other hand, the crystal-field Hamiltonian parameters (B_q^k and G_{10A}^4) determined from our analyses show some significant variations among the three systems, which may be attributed to differences between the *anisotropic* parts of the $4f$-electron crystal-field interactions operative in the different systems. These host-dependent parameter variations provide insight into the microscopic structural environment of the Er^{3+} ions in the different garnets.

The introduction of two-electron correlation crystal-field (CCF) interaction terms into the model Hamiltonian produced only modest improvements in the *overall* rms deviations of our calculated-versus empirical energy-level data fits (see Table I). However, inclusion of the $G_{10AQ}^4 \hat{g}_{10AQ}^{(4)}$ CCF terms [as shown in Eq. (5)] produced dramatically improved agreement between calculated and experimentally observed *crystal-field splitting energies* within several J-multiplet manifolds (see Table III). Two of these multiplets, $^2H(2)_{11/2}$ and $^2H(2)_{9/2}$, were specifically targeted for CCF treatment (by making an informed choice of CCF operators) because their crystal-field splittings were particularly resistant to fits based on any reasonable one-electron crystal-field parametrization (B_q^k) scheme. Crystal-field splittings calculated for two other multiplets, $^4I_{11/2}$ and $^4G_{11/2}$, were also strongly influenced by our chosen CCF operators, largely because the LS parentages of these multiplets bear a close resemblance to the LS parentage of $^2H(2)_{11/2}$. The use of specific CCF operators to resolve crystal-field splitting problems within particular J-multiplet manifolds has been employed previously in energy-level analyses of Nd^{3+}, Gd^{3+}, and Ho^{3+} systems,[30,45] and of Tb^{3+} systems.[48] The CCF analyses carried out in this study have close parallels with those carried out by Li and Reid[30] for the problematic $^2H(2)_{11/2}$ multiplet of Nd^{3+} systems.

The analyses carried out in this study focused entirely on the *locations* of crystal-field energy levels and on crystal-field splittings within J-multiplet manifolds. All of the energy levels are Kramers doublets with identical symmetry properties in the D_2 double group. The *eigenvalues* of the parametrized Hamiltonians derived from our analyses fit the experimental energy-level data quite well. However, it is important to note that the available experimental data contain no information about the JM_J compositions of the crystal-field wave functions, and, therefore, cannot be used to determine the quality of the *eigenvectors* associated with the model Hamiltonians. In our analyses, comparisons between calculation and experiment are based strictly on energy-level locations, and definitive conclusions regarding the $SLJM_J$ compositions of crystal-field state vectors cannot be drawn. Detailed analyses of the state vectors must await measurements of magneto-optical and magnetic g-tensor properties, and, possibly, quantitative optical line-strength data. Transition probabilities of optical absorption and emission processes are of particular interest, and reliable calculations of these properties require highly accurate state vectors.[49–53] However, for noncentrosymmetric systems, these calculations also require rather detailed information about (*or* well-characterized parametric representations of) *odd-parity* crystal-field interactions that can couple the $4f$ (optical) electrons to the electric-dipole components of a radiation field. Some success has been achieved in performing such calculations for Nd^{3+} in YAG,[54] but calculations for the Er^{3+}:garnet systems have not yet been attempted.

ACKNOWLEDGMENTS

The authors wish to thank M. Kokta (Union Carbide) and M. Randles (Litton Airton) for supplying the garnet crystals used in this study. J.B.G. wishes to thank the Office of Naval Technology for its support. The work carried out at the University of Virginia was supported by the National Science Foundation (NSF Grant No. CHE-9213473 to F.S.R.). S.B.S. wishes to acknowledge the National Research Council for its support of her work while at the Harry Diamond Laboratories and support from the Optical and Discharge Physics Group at the University of Illinois under ONR Grant No. (N00014-90-J4095). T.H.A. wishes to thank the U.S. Army Night Vision and Electro-Optics Directorate for its financial support.

*Current address: Department of Physics and Astronomy, University of Canterbury, Christchurch, New Zealand.

†Current address: University of Illinois, Gaseous Electronics Laboratory, 607 East Healey Street, Champaign, Illinois 61802.

[1]W. F. Krupke and J. B. Gruber, J. Chem. Phys. **41**, 1225 (1964).

[2]R. L. Remski, L. T. James, K. H. Gooen, B. DiBartolo, and A. Ling, IEEE J. Quantum Electron. **5**, 214 (1969).

[3]Yu. K. Voronko and V. A. Sychugov, Phys. Status Solidi **25**, K119 (1968).

[4]L. F. Johnson and H. J. Guggenheim, Appl. Phys. Lett. **20**, 474 (1972).

[5]A. A. Kaminskii, Izv. Akad. Nauk. SSSR, Neorg. Mater. **7**, 904 (1971).

[6]A. A. Kaminskii, A. A. Pavlyuk, P. V. Klevtsov, I. F. Balashov, V. A. Berenberg, S. E. Sarkisov, V. A. Fedorov, M. V. Petrov, and V. V. Lubchenko, Izv. Akad. Nauk. SSSR, Neorg. Mater. **13**, 582 (1977).

[7]Z. S. Saidov, V. A. Smirnov, and I. A. Shcherbakov, Kvan. Elektron. (Moscow) **15**, 497 (1988) [Sov. J. Quantum Electron. **18**, 313 (1988)].

[8]S. A. Pollack and D. B. Chang, J. Appl. Phys. **64**, 2885 (1988).

[9]G. J. Kintz, R. Allen, and L. Esterowitz, Appl. Phys. Lett. **54**, 681 (1989).

[10]F. Auzel, S. Hubert, and D. Meichenin, Appl. Phys. Lett. **54**,

681 (1989).
[11]S. B. Stevens, C. A. Morrison, T. H. Allik, A. L. Rheingold, and B. S. Haggerty, Phys. Rev. B **43**, 7386 (1991).
[12]J. A. Hutchinson and T. H. Allik, Appl. Phys. Lett. **60**, 1424 (1992).
[13]B. J. Dinerman and P. F. Moulton (unpublished).
[14]S. A. Pollack, D. B. Chang, and N. L. Moise, J. Appl. Phys. **60**, 4077 (1986).
[15]O. L. Malta, E. Antic-Fidancev, M. Lemaître-Blaise, J. Dexpert-Ghys, and B. Piriou, Chem. Phys. Lett. **129**, 557 (1986).
[16]T. Y. Fan, G. L. Dixon, and R. L. Byer, Opt. Lett. **11**, 204 (1986).
[17]A. J. Silversmith, W. Lenth, and R. M. Macfarlane, Appl. Phys. Lett. **51**, 1977 (1987).
[18]T. Y. Fan and R. L. Byer, J. Opt. Soc. Am. B **3**, 1519 (1986).
[19]R. A. McFarlane, Opt. Lett. **16**, 1397 (1991).
[20]W. F. Krupke, *Compact Blue-Green Lasers Technical Digest 1992* (Optical Society of America, Washington, DC, 1992), Vol. 6, ThB2, p. 14.
[21]J. B. Gruber, *Tunable Lasers for Engineering and Biological Applications* (SPIE, Bellingham, WA, 1992).
[22]R. C. Stoneman and L. Esterowitz, Opt. Lett. **15**, 486 (1990).
[23]G. H. Rosenblatt, R. C. Stoneman, and L. Esterowitz, in *OSA Proceedings of Advanced Solid-State Lasers,* edited by H. P. Jenssen and G. Dube (Optical Society of America, Washington, DC, 1991), Vol. 6, p. 26.
[24]A. A. Kaminskii, *Laser Crystals* (Springer, Berlin, 1981).
[25]C. A. Morrison and R. P. Leavitt, in *Spectroscopic Properties of Triply Ionized Lanthanides in Transparent Host Crystals,* Handbook on the Physics and Chemistry of Rare Earths, Vol. 5, edited by K. A. Gschneidner, Jr. and L. Eyring (North-Holland, Amsterdam, 1982).
[26]P. F. Moulton, J. G. Manni, and G. A. Rines, IEEE J. Quantum Electron. **24**, 960 (1988).
[27]M. Kh. Ashurov, Yu. K. Voronko, V. V. Osiko, A. A. Sobol, B. P. Starikov, M. I. Timoshechkin, and A. Ya. Yablonskii, Phys. Status Solidi A **35**, 645 (1976).
[28]N. P. Agladze, Kh. S. Bagdasarov, E. A. Vinogrodov, V. I. Zhekov, T. M. Murina, M. N. Popova, and E. A. Fedrov, Kristallografiya **33**, 912 (1988) [Sov. Phys. Crystallogr. **33**, 540 (1988)].
[29]J. B. Gruber, M. E. Hills, M. D. Seltzer, G. A. Turner, and C. A. Morrison, Chem. Phys. **144**, 327 (1990).
[30]C. L. Li and M. F. Reid, Phys. Rev. B **42**, 1903 (1990).
[31]J. B. Gruber, M. E. Hills, T. H. Allik, C. K. Jayasankar, J. R. Quagliano, and F. S. Richardson, Phys. Rev. B **41**, 7999 (1990).
[32]J. R. Quagliano, F. S. Richardson, and M. F. Reid, J. Alloys Compounds **180**, 131 (1992).
[33]S. Geller, Z. Kristallogr. **125**, 1 (1967).
[34]M. Kokta, J. Solid State Chem. **8**, 39 (1973).
[35]C. D. Brandle and R. L. Barns, J. Cryst. Growth **20**, 1 (1973).
[36]J. B. Gruber, M. D. Seltzer, M. E. Hills, S. B. Stevens, and C. A. Morrison, J. Appl. Phys. **73**, 1929 (1993).
[37]C. A. Morrison, J. B. Gruber, and M. E. Hills, Chem. Phys. **154**, 437 (1991).
[38]J. B. Gruber, M. E. Hills, C. A. Morrison, G. A. Turner, and M. R. Kokta, Phys. Rev. B **37**, 8564 (1988).
[39]F. Euler and J. A. Bruce, Acta Crystallogr. **19**, 971 (1965).
[40]T. H. Allik, C. A. Morrison, J. B. Gruber, and M. R. Kokta, Phys. Rev. B **41**, 21 (1990).
[41]G. B. Lutts, A. L. Denisov, E. V. Zharikov, A. I. Zagumenngi, S. N. Kozlikin, S. V. Lavrishchev, and S. A. Samoylova, Opt. Quant. Electron. **22**, S269 (1990).
[42]W. T. Carnall, G. L. Goodman, K. Rajnak, and R. S. Rana, J. Chem. Phys. **90**, 3443 (1989).
[43]C. A. Morrison, *Angular Momentum Theory Applied to Interactions in Solids* (Springer, Berlin, 1988).
[44]B. R. Judd, J. Chem. Phys. **66**, 3163 (1977).
[45]M. F. Reid, J. Chem. Phys. **87**, 2875 (1987).
[46]W. T. Carnall, P. R. Fields, and K. Rajnak, J. Chem. Phys. **49**, 4424 (1968).
[47]K. A. Schoene, J. R. Quagliano, and F. S. Richardson, Inorg. Chem. **30**, 3803 (1991).
[48]J. P. Bolender, J. R. Quagliano, and F. S. Richardon (unpublished).
[49]P. S. May, M. F. Reid, and F. S. Richardson, Mol. Phys. **61**, 1471 (1987).
[50]P. S. May, C. K. Jayasankar, and F. S. Richardson, Chem. Phys. **138**, 139 (1989).
[51]D. M. Moran and F. S. Richardson, Phys. Rev. B **42**, 3331 (1990).
[52]E. M. Stephens, D. H. Metcalf, M. T. Berry, and F. S. Richardson, Phys. Rev. B **44**, 9895 (1991).
[53]M. F. Reid, J. Chem. Phys. **87**, 6388 (1988).
[54]M. F. Reid, C. K. Jayasankar, and F. S. Richardson (unpublished).